Detection of Ion Plasma Waves by Collective Thomson Scattering

B. S. Bauer,[1] R. P. Drake,[1] K. G. Estabrook,[1] R. G. Watt,[2] M. D. Wilke,[2] and S. A. Baker[3]

[1]*Lawrence Livermore National Laboratory, Livermore, California 94551*

[2]*Los Alamos National Laboratory, Los Alamos, New Mexico 87545*

[3]*EG&G—Los Alamos Operations, Los Alamos, New Mexico 87544*

(Received 11 October 1994)

The first unambiguous experimental detection of ion plasma waves is reported. These short-wavelength ($k\lambda_{De} > 1$), purely electrostatic ion waves were first predicted by Tonks and Langmuir in 1929. The waves are observed in a long-scalelength ($L > 10^4/k$), multiply ionized ($Z = 22$), laser-produced plasma. The frequency (ω), wave number (k), and amplitude evolution of the ion waves are measured by time-resolved spectroscopy of the scattering from the ion waves of a probe laser beam. The wave frequency is approximately the ion plasma frequency (ω_{pi}) when $k\lambda_{De}$ exceeds 1, as predicted by the theoretical dispersion relation.

PACS numbers: 52.35.Fp, 52.40.Nk

Understanding the dynamical behavior of a medium requires thorough knowledge of all its waves. A plasma, consisting of multiple species of freely moving charged particles, sustains a richer spectrum of waves than does any other medium. A number of waves theoretically postulated to exist in plasmas have not yet been experimentally observed. One such wave, whose dispersion relation was originally derived by Tonks and Langmuir [1] in 1929, has eluded clear detection for 65 years. In this Letter, we report the first unambiguous experimental observation of this wave, the ion plasma wave.

An ion plasma wave (IPW) is a purely electrostatic wave, with a propagation vector parallel to the ambient magnetic field, if any, in which ion fluid elements oscillate about a relatively uniform electron background. This is in contrast to the fluid motion in an ion acoustic wave (IAW), in which ions and electrons oscillate together, and it occurs when the ion density modulation is of such short wavelength that plasma electrons do not effectively shield it. The ion plasma wave is named by analogy to the electron plasma wave (the Langmuir wave), in which electron fluid elements oscillate about a uniform ion background. A common feature of such nonquasineutral waves is that the wave frequency approaches a resonant value that depends only on the plasma parameters. For the IPW, this resonant frequency is the ion plasma frequency $\omega_{pi} = (4\pi Zne^2/M)^{1/2}$. Here Z is the ionization state of the ions, n is the plasma electron density, e is the electron charge, and M is the ion mass. We have measured the frequency of the IPW as a function of n and find that it follows ω_{pi}.

IPWs are important in plasmas with high ZT_e/T_i, where they are weakly damped. Here T_e and T_i are the electron and ion temperatures, respectively. Examples of such plasmas include the multiply ionized ($Z \gg 1$) plasmas used in x-ray lasers and inertial confinement fusion (ICF), and some of the gas-discharge plasmas used for semiconductor processing. In some ICF regimes [2], IPWs can participate in stimulated scattering, as observed here. More generally, ion wave nonlinearities transfer ion wave energy to higher wave numbers, and thereby shift the turbulent ion wave spectrum into the IPW domain.

The first pioneering attempts to observe IPWs, driven by an oscillating potential on a wire-mesh grid in a singly ionized ($Z = 1$) plasma, detected ballistic pseudowaves instead [3]. Two later experiments [4], in Q-machine plasmas, succeeded in observing nonballistic ion waves at frequencies above ω_{pi}. However, these were heavily damped ion kinetic modes, not IPWs. The wave phase velocity was approximately the ion thermal speed, and ω_{pi} was not resonant. Most recently, using a double plasma device, Armstrong [5] made an inconclusive observation of IPWs. Given the proximity of the receiving probe to the central grid for these observations, the intriguing, rapidly decaying probe signals likely represent modulated streaming ions or a kinetic mode of the combined system of central grid and probe sheaths, rather than a plasma wave.

Our experiment succeeds in unambiguously detecting IPWs by employing laser-based methods of ion wave detection and plasma production. Plasma-immersed solid diagnostics are avoided by using resonant laser scattering [6] to measure the ion wave frequency and wave number. *Undriven* or *optically driven* [7] ion waves are detected, eliminating plasma-immersed solid wave drivers. A laser-produced, multiply ionized ($Z = 22$) copper ($M = 63.5$ amu) plasma is employed, with $ZT_e/T_i \approx 30$ and no neutral atoms or fast ion impurities, to obtain weak IPW damping ($\gamma \approx 10^{-2}\omega_{pi}$ predicted, Fig. 1).

The dispersion relation for electrostatic ion waves in infinite, uniform, unmagnetized, weakly coupled plasma [11] is

$$\omega^2 = \frac{\omega_{pi}^2}{1 + (k\lambda_{De})^{-2}} + 3v_{th_i}^2 k^2, \tag{1}$$

$$\frac{\gamma}{\omega} = \sqrt{\pi}\,\zeta^3\left(e^{-\zeta^2} + \frac{T_i v_{th_i}}{ZT_e v_{th_e}}\right). \tag{2}$$

 0031-9007/95/74(18)/3604(4)$06.00

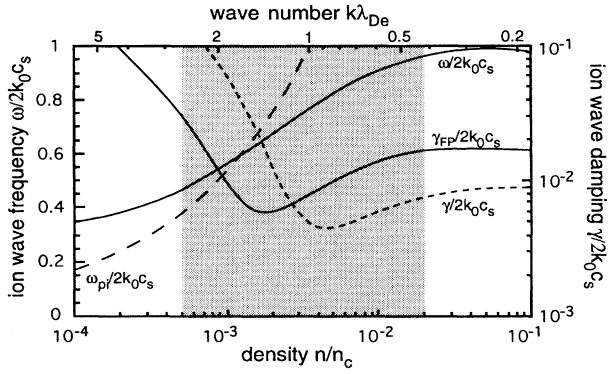

FIG. 1. Theoretical ion wave frequency ω and damping γ as a function of plasma density n, for parameters of the experiment [$k = 2k_0(1 - n/n_c)^{1/2}$, laser critical density $n_c = 4.02 \times 10^{21}$ cm^{-3}, $k_0 = 2\pi/0.5265$ μm, $Z = 22$, $M = 63.5$ amu, $T_e = 450$ eV, and $T_i = 290$ eV; the values of T_e and T_i correspond to the temperatures at $n \approx 2 \times 10^{-3} n_c$ in the experiment]. ω decreases by a factor of 2 as n is decreased through the range experimentally probed (shown shaded), from $2 \times 10^{-2} n_c$ to $5 \times 10^{-4} n_c$. The normalized wave number $k\lambda_{De}$ is shown in parallel to n/n_c; its approximate reciprocal, $\omega_{pi}/2k_0c_s$, where $c_s \equiv \lambda_{De}\omega_{pi} = (ZT_e/M)^{1/2}$, is also plotted with respect to the left ordinate. The ion wave frequency ($\omega/2k_0c_s$) and collisionless damping are obtained from Eqs. (1) and (2). Ion-ion collisions increase the wave damping $\gamma/2k_0c_s$ (by 0.0003 [for $k\lambda_{ii} = 20$ at $n = 10^{-4}n_c$] to 0.01 [for $k\lambda_{ii} = 0.2$ at $n = 10^{-1}n_c$]) [8,9]; the combined collisional and collisionless damping $\gamma_{FP}/2k_0c_s$ is calculated from a computational form [10] to numerical solutions of the linearized Fokker-Planck equation.

Here ω, γ, and k are the ion wave frequency, damping, and wave number, respectively; $\zeta^2 = \frac{3}{2} + ZT_e/[2T_i(1 + k^2\lambda_{De}^2)]$, $\lambda_{De} = (T_e/4\pi ne^2)^{1/2}$ is the electron Debye shielding length; $v_{th_i} = (T_i/M)^{1/2}$ and $v_{th_e} = (T_e/m)^{1/2}$ are the ion and electron thermal speeds, respectively; and m is the electron mass. This dispersion relation includes both IAWs and IPWs. The familiar IAW has $k\lambda_{De} \ll 1$, so $\omega \approx \omega_{pi}k\lambda_{De} = c_sk$, where $c_s \equiv \lambda_{De}\omega_{pi} = (ZT_e/M)^{1/2}$ is the ion acoustic sound speed (defined here as the IAW phase velocity in the limit as $T_i \to 0$ and $k\lambda_{De} \to 0$). In this case, the charge-density fluctuations of the electrons and ions nearly cancel, and the residual difference is proportional to the fluctuation of the electron pressure. The resulting nondispersive behavior is typical of pressure-driven modes. In contrast, the IPW has a short wavelength [$1 < k\lambda_{De} \lesssim (ZT_e/3T_i)^{1/2}$], so $\omega \approx \omega_{pi}$. The electrons are unable to shield the ion charge fluctuation, and the resulting dispersive behavior is typical of nonquasineutral modes. The ion Landau damping of this wave is weak only when $ZT_e/T_i \gg 1$.

In the experiment, the ion wave is observed at a series of plasma densities by varying the location of the laser probe along the plasma density profile. The wave number of the ion wave probed is fixed, by the laser backscatter process, at twice the wave number of the laser probe. The ion wave probed is predicted (Fig. 1) to go from the IAW regime ($k\lambda_{De} = kc_s/\omega_{pi} < 1$) to the IPW regime ($k\lambda_{De} = kc_s/\omega_{pi} > 1$), as the density probed is decreased, with all else held constant. When the plasma density is high, $\omega_{pi} > kc_s$ and $\omega \approx kc_s$. As the density decreases, ω_{pi} drops below kc_s and clamps the ion wave frequency at $\omega \approx \omega_{pi}$.

A long-scale plasma was developed for the experiment, in which the density dependence of the ion wave frequency could be observed, unclouded by Doppler shifts, nonuniform density, or ion species inhomogeneity [12]. The experiment (Fig. 2) utilizes the Trident laser facility [13] at Los Alamos National Laboratory. The plasma is produced by two consecutive 2.2 ns FWHM temporal-flat-top laser pulses focused (through $f/6$ lenses of 1200 mm focal length) on a planar, solid, copper target. The laser light from each beam (150 J on target, at wavelength 0.5265 μm) is distributed (with a characteristic peak intensity of 3×10^{13} W/cm^2) along a line focus 2.1 mm long by a 0.11 mm wide (FWHMs). The line focus is produced by passing the two laser beams through random phase plates whose elements consist of long (250 mm), narrow (0.635 mm) strips. The beams are also passed through tent-wedge biprisms that split them into two halves with milliradian pointing separation. This yields a double-peaked intensity profile along the line focus. The spatial distribution of laser intensity determines the flow of the plasma ablating from the target. Before

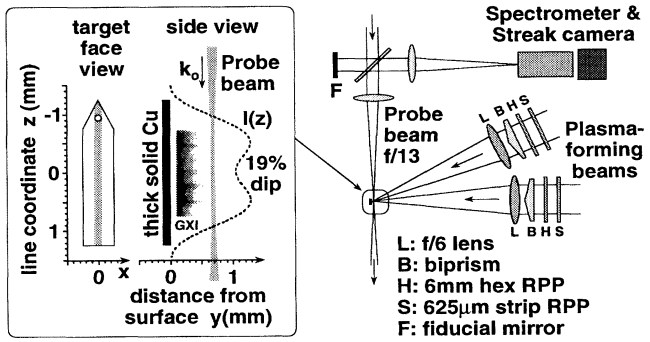

FIG. 2. Experimental schematic. The stripe down the center of the target (face view) is the plasma-forming line focus. The hole in the target is for alignment, and the pointed end, pointed toward the probe beam source, reduces stray probe beam backscatter reflections from the target. When the intensity profile along the line focus [$I(z)$] has a dip in the center of 19%, the plasma expansion is predominantly perpendicular to the target surface, resulting in narrowband collective Thomson backscattering of the probe beam. The plasma stream lines are captured in the 80 ps gated x-ray image of the central portion ($-0.75 < z < 0.75$, $0.1 < y < 0.6$) of the plasma. The light regions in between the dark streams are regions containing beryllium (Be) entrained in the copper (Cu) plasma, from Be deposited on the surface of the Cu target. Ion wave measurements were made on subsequent shots in pure Cu plasmas (no Be).

performing the ion wave measurements, the plasma flow lines were observed with gated 80 ps x-ray images of the expanding plasma, using copper targets embedded with beryllium microdots. The depth of the intensity dip in the line-focus intensity profile (between the two intensity peaks) was specifically adjusted to yield plasma flow lines predominately perpendicular to the target surface.

The line-focus irradiation pattern produces a quasicylindrical plasma, with a plasma density gradient in the direction normal to the target surface, and a relatively uniform density along the length of the line focus, at a given distance from the target surface. The plasma density profile expansion is measured with time-resolved (130 ps), holographic laser interferometry (at wavelength 0.263 μm), and by the refraction of the probe beam. The plasma is in quasi-steady-state $[n(\partial n/\partial t)^{-1} > 2$ ns $> 10^3\omega_{pi}^{-1}]$ by the end of the 4.4 ns plasma-production laser pulse. At the center of the line focus, the density profile lies between $0.020n_c \exp(-y/0.41)$ and $0.037n_c \exp(-y/0.50)$, for y, the distance from the target in mm, between 0.3 and 1.5 mm. The plasma density is constant to within $\pm 10\%$ along the central 2 mm of the line focus. An ion spectrometer observes the spectrum of ionization states to consist predominantly of $Z = 19$ to $Z = 25$, with average ionization $\overline{Z} = 22 \pm 2$, and spread $\Delta Z_{\rm rms} = 1.5 \pm 0.5$. The presence of the mix of ionization states shifts ω_{pi} by $<1\%$, permitting the use here of a single-species analysis with $Z = \overline{Z}$. The plasma sound speed $[c_s \equiv (ZT_e/M)^{1/2} = 0.144 \pm 0.011$ mm/ns] is obtained, at plasma densities $n \geq 0.01n_c$, from time-resolved spectroscopy of the collective Thomson sidescattering of the plasma-production and probe laser beams from IAWs. Factoring $Mc_s^2 = (\overline{Z} = 22 \pm 1.4)(T_e = 620 \pm 50$ eV) yields the electron temperature (here Cu ionization levels have been used to correlate changes in $\overline{Z}$ with changes in T_e). LASNEX [14] 2D computer simulations yield plasma parameters in reasonable agreement with the observations, and permit us to estimate the ion temperature T_i and the temperature gradients. $T_i(y) = (500 \pm 40$ eV$)[1 - (y - 0.44)/2]$ for $0.44 \leq y \leq 1.5$ mm, and is approximately constant for $0.3 \leq y \leq 0.44$ mm. The electron temperature decreases gradually as $\exp(-y/2.5)$ for $0.44 \leq y \leq 1.5$ mm, and is approximately constant for $0.3 \leq y \leq 0.44$ mm. The ionization state $\overline{Z}$ is very uniform throughout the plasma $(\Delta\overline{Z} < 1)$.

A laser probe beam (0.35 ns FWHM Gaussian, 20 J, 0.5265 μm, $f/13$, 7×10^{14} W/cm^2) is injected into the plasma, parallel to the surface of the target, to scatter from ion waves. The brief probe pulse transects the plasma before the end of the plasma-production pulse (the probe beam peaks 0.50 ns before the last plasma-production beam turns off). The probe beam propagates along the line focus, offset from the target by a distance chosen to produce scattering from ion waves at a known plasma density. We measured the ion wave frequency, at known wave numbers, with time-resolved spectroscopy (typical resolutions $\Delta\lambda = 0.8$ Å, $\Delta t = 0.03$–0.23 ns) of the scattered light. This light $(\mathbf{k}_s, \omega_s)$ is generated by the beating of the probe laser $(\mathbf{k}_p, \omega_0)$ with the ion waves $(\mathbf{k}, \omega)$, and has frequency $\omega_s = \omega_0 \pm \omega$. The scattering geometry is chosen so that the wave vectors, of the ion waves which scatter the probe laser into the detector, are parallel to the target surface, and hence perpendicular to the plasma flow. That is, $\mathbf{k} \cdot \mathbf{u} = \pm(\mathbf{k}_p - \mathbf{k}_s) \cdot \mathbf{u} \approx 0$, where $\mathbf{u}$ is the ion flow velocity. This yields narrowband scattering of the probe laser, with small Doppler shifting and Doppler broadening of the frequency spectrum. The densities probed in this experiment were sufficiently low that the wave numbers of the electromagnetic waves in the plasma were within 1% of those in vacuum. The refraction of the probe laser was measured by observing the location of the beam, with burn paper, at the probe-beam exit port of the vacuum vessel; it was no more than a few degrees for the results reported here. The probe beam is observed not to heat the plasma appreciably.

One of the IPW observations is shown in Fig. 3. The backscatter spectrum contains three signals: a blueshifted unstimulated collective Thomson scatter peak, from ion waves propagating counter to the probe laser; a redshifted stimulated-scatter peak, from ion waves propagating in the same direction as the probe laser; and an unshifted wavelength, timing, and intensity fiducial. The redshifted and blueshifted peaks are separated by only 4.3 Å, or 40% of the IAW separation observed at higher density. This and the plasma parameters given above imply that the ion waves are in the IPW regime, with $k\lambda_{\rm De} = 2.3 \pm 0.2$.

The ion wave frequency, at wave number $k \approx 2k_0$, was measured at a series of plasma densities to observe the

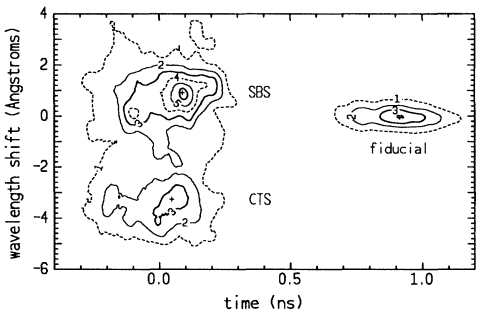

FIG. 3. A time-resolved spectrum of light backscattered from ion plasma waves ($k\lambda_{\rm De} = 2.3 \pm 0.2$) at low density ($n = 6 \times 10^{-4}n_c$). Contours represent 10 W/Å increases in the spectral power of the backscattered signal. The ordinate is the shift of the wavelength from the laser wavelength, with the origin obtained from the fiducial signal at late time. The spectral resolution is 0.8 Å; the temporal resolution is 0.23 ns. 100 nJ of light was backscattered into the observed spectral range, or 5×10^{-9} of the 22 J of incident probe laser energy. The probe laser was 1.50 mm from the target surface.

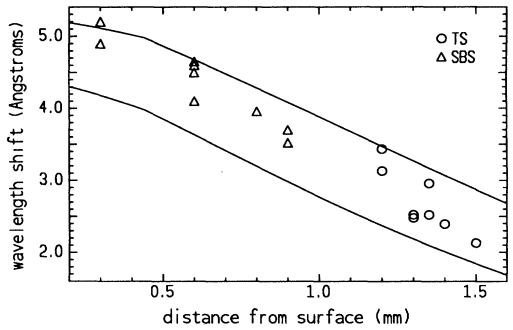

FIG. 4. The measured ion wave frequencies are in agreement with the dispersion relation. Backscatter spectral shift versus probe beam position. Circles represent backscatter in which both the stimulated and unstimulated signals are visible. In this case, the spectral shift is half the spectral separation between the two peaks, a quantity independent of the overall Doppler shift (-0.4 ± 0.6 Å). Triangles represent data from spectra in which the stimulated signal is very strong, and the unstimulated signal is not observed because the entire backscatter signal was intensionally attenuated. In this case, the spectral shift includes a small unknown Doppler shift (expected to fall within the observed range above). All the data points come from unsaturated streak camera images with a high signal-to-noise ratio. The spatial resolution is limited by the pointing accuracy (0.01–0.05 mm) and the best-focus diameter (0.10 mm) of the probe laser. The two curves represent the maximum and minimum spectral shifts predicted by the ion wave dispersion relation [Eq. (1)] for the plasma parameters described in the text. The observed shifts fall within the predicted range.

transition from the IAW to the IPW regime. Figure 4 shows the dependence of the backscattered spectral shift on the distance of the probe laser from the target surface. Also shown are the shifts predicted by the ion wave dispersion relation [Eq. (1)] for the plasma profiles and parameters described above. The upper curve shows the maximum predicted shift; it assumes that a high density resulted from rapid plasma expansion, caused by high plasma temperatures and ionization state. The lower curve, the minimum predicted shift, shows the wavelength shift for the low plasma parameters. The measured spectral shifts lie between the two curves and thus are in agreement with the dispersion relation. The measured density profile accounts for over 80% of the variation of ion wave frequency with position, and, at low densities, the $\omega \approx \omega_{pi}$. Other factors, such as spatial temperature variations, cannot account for a frequency change as large as that observed. This clearly represents the observation of IPWs, and verification of the IPW dispersion relation.

The observation of IPWs serves as a reminder that λ_{De} is not the smallest relevant scale for all plasmas. In particular, particle-in-cell computer simulations of high-ZT_e/T_i plasmas should consider employing sub-λ_{De} grid spacings. Indeed, even for singly ionized plasmas, computer simulations of the electron-ion drift instability have found inclusion of small-scale structures ($k\lambda_{De} > 1$) essential to a correct description of the plasma turbulence [15]. In addition, although a completely smoothed phase-space description of the plasma adequately describes the measurements reported here, examination of sub-λ_{De} structures may ultimately yield information on the effects of particle granularity and collisions on plasma phenomena.

We thank R. Griffith for his work with the streak camera; S. Dixit and I. Thomas for producing the random phase plates; T. Hurry and J. Faulkner for their efforts in the target area; H. Bush, P. Gobby, V. Gomez, J. Moore, R. Manzanares, and R. Henneke for producing and metrologizing the targets; R. Johnson, J. Goddard, S. Reading, F. Archuleta, and N. Okamoto for modification and operation of the laser; and B. Afeyan, T. Shepard, J. Cobble, M. Goldman, and A. Rubenchik for valuable discussions of laser plasma interactions, x-ray spectroscopy, and ion wave dynamics. This work was performed under the auspices of the U.S. Department of Energy by the Lawrence Livermore National Laboratory under Contract No. W-7405-ENG-48 and by the Los Alamos National Laboratory.

[1] L. Tonks and I. Langmuir, Phys. Rev. **33**, 195 (1929).
[2] W. L. Kruer, in *Laser Interaction and Related Plasma Phenomena,* edited by George H. Miley (Plenum Press, Ne York, 1991).
[3] W. D. Jones, H. J. Doucet, and J. M. Buzzi, *An Introduction to the Linear Theories and Methods of Electrostatic Waves in Plasmas* (Plenum Press, New York, 1985).
[4] N. Sato, H. Ikezi, Y. Yamashita, N. Takahashi, and T. Obiki, Phys. Lett. **26A**, 333 (1968); H. J. Doucet and D. Gresillon, Phys. Fluids **13**, 773 (1970).
[5] R. J. Armstrong, Plasma Phys. Controlled Fusion **28**, 1569 (1986).
[6] John Sheffield, *Plasma Scattering of Electromagnetic Radiation* (Academic Press, New York, 1975).
[7] William L. Kruer, *The Physics of Laser Plasma Interactions* (Addison-Wesley, New York, 1988).
[8] C. J. Randall, Phys. Fluids **25**, 2231 (1982).
[9] V. Yu. Bychenkov, J. Myatt, W. Rozmus, and V. T. Tikhonchuk, Phys. Plasmas **1**, 2419 (1994).
[10] M. Casanova, Laser Part. Beams **7**, 165 (1989).
[11] Dwight R. Nicholson, *Introduction to Plasma Theory* (Wiley, New York, 1983); D. G. Swanson, *Plasma Waves* (Academic Press, San Diego, 1989).
[12] B. S. Bauer, R. P. Drake, K. G. Estabrook, J. F. Camacho, R. G. Watt, M. D. Wilke, G. E. Busch, S. E. Caldwell, and S. A. Baker, Phys. Plasmas (to be published).
[13] R. G. Watt, Rev. Sci. Instrum. **64**, 1770 (1993).
[14] G. B. Zimmerman and W. L. Kruer, Comments Plasma Phys. Controlled Fusion **2**, 51 (1975).
[15] R. H. Berman, D. J. Tetreault, and T. H. Dupree, Phys. Fluids **28**, 155 (1985).